Electronic Supplementary Information for

One-dimensional alignment of strong Lewis acid sites in a porous coordination polymer

Takashi Kajiwara,[a] Masakazu Higuchi,[b] Akihiro Yuasa,[a] Hideyuki Higashimura,*[a] and Susumu Kitagawa*[bc]

[a] Advanced Materials Research Laboratory, Sumitomo Chemical Co., Ltd., 6 Kitahara, Tsukuba, Ibaraki 300-3294, Japan.
[b] Institute for Integrated Cell-Material Sciences (iCeMS), Kyoto University, Yoshida Ushinomiyacho, Sakyo-ku, Kyoto 606-8501, Japan.
[c] Department of Synthetic Chemistry and Biological Chemistry, Graduate School of Engineering, Kyoto University, Kyoto-daigaku Katsura, Nishikyo-ku, Kyoto 615-8510, Japan.

higashimura@sc.sumitomo-chem.co.jp
kitagawa@icems.kyoto-u.ac.jp

Experimental Section

General Remarks. ^{1}H NMR (500 MHz) and ^{13}C NMR (125 MHz) spectra were recorded on a JEOL JNM-A500 spectrometer. The ^{1}H NMR chemical shifts are reported in ppm downfield from tetramethylsilane (δ scale) and referenced to the internal residual DMSO-d_5 (2.50 ppm). The ^{13}C NMR chemical shifts are reported in ppm downfield from tetramethylsilane (δ scale) and referenced to the carbon-13 signals of DMSO-d_6 (39.52 ppm). Multiplicity of signals in ^{13}C NMR spectra was determined by DEPT technique. Mass spectra were recorded on a Thermo Fisher Scientific EXACTIVE spectrometer. Thermogravimetric analyses (TGA) were performed on a RIGAKU Thermo plus EVO II TG8120, using a heating rate of 5 K min^{-1} under an N_2 atmosphere. X-ray powder diffraction (XRPD) data were collected on a Bruker AXS D8 DISCOVER with GADDS. Data were collected over the 2θ range from 4.00° to 40.20° in 0.02° steps via 600 sec scans, with Cu Kα radiation (λ = 1.54184 Å). Gas sorption isotherm measurements were performed with a BEL Japan BELSORP-max. IR spectra were recorded on a Thermo Fisher Scientific Nicolet 6700 spectrometer.

Materials. All reagents and solvents used for the syntheses of ligand H_3BTTc and PCPs are commercially available and were used as received without further purification. MIL-101(Cr)[S1] and MIL-103(La)[S2] were synthesized and activated according to procedures reported in the literature. ZIF-8[S3] was purchased from Sigma-Aldrich (Basolite® Z1200).

Synthesis of H_3BTTc. Under an N_2 atmosphere, the mixture of tribromobenzene (2.36 g, 7.51 mmol), 5-carboxythiophene-2-boronic acid (12.9 g, 75.0 mmol), K_2CO_3 (15.6 g, 113 mmol), $Pd(PPh_3)_4$ (870 mg, 0.752 mmol), and 3:1 (v:v) DMF/H_2O (300 mL) was heated at 100 °C for 48 h. After cooling to room temperature, insoluble materials were removed by filtration. To the filtrate were added H_2O and $CHCl_3$, and the aqueous layer was extracted with water. To the resultant aqueous solution was added HClaq to give white precipitates. Filtration and washing successively with H_2O, EtOH, and $CHCl_3$ afforded the desired tricarboxylic acid H_3BTTc (3.10 g, 6.79 mmol, 90%). ^{1}H NMR (DMSO-d_6): δ 7.76 (d, $^{3}J_{HH}$ = 4.0 Hz, 3H), 7.83 (d, $^{3}J_{HH}$ = 4.0 Hz, 3H), 7.97 (s, 3H), 13.0 (br s, 3H). ^{13}C NMR (DMSO-d_6): δ 123.16 (d), 126.29 (d), 134.28 (d), 134.35 (s), 134.88 (s), 147.92 (s), 162.76 (s). HRMS-ESI (*m*/*z*): $[M–H]^-$ calcd for $C_{21}H_{11}O_6S_3$, 454.9723; found 454.9736. The ^{1}H and ^{13}C NMR spectra are shown in Fig. S1 and S2.

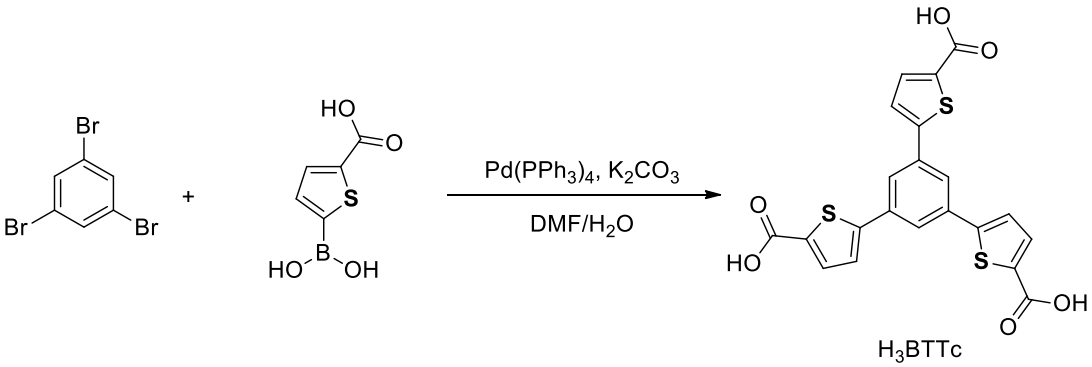

Scheme S1 Synthesis of a new thiophene-based tritopic organic linker H_3BTTc.

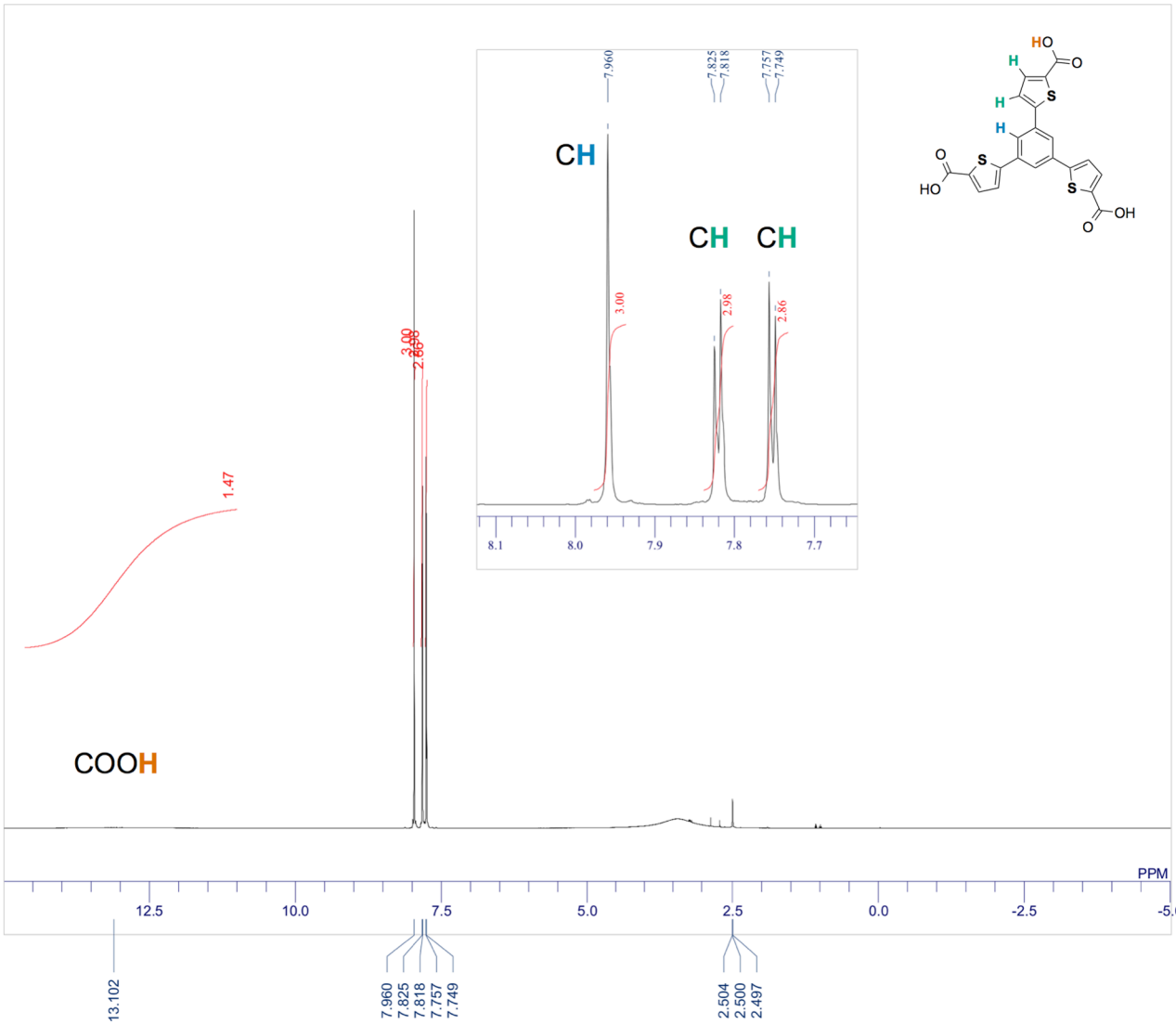

Fig. S1 ^{1}H NMR spectrum of H_3BTTc.

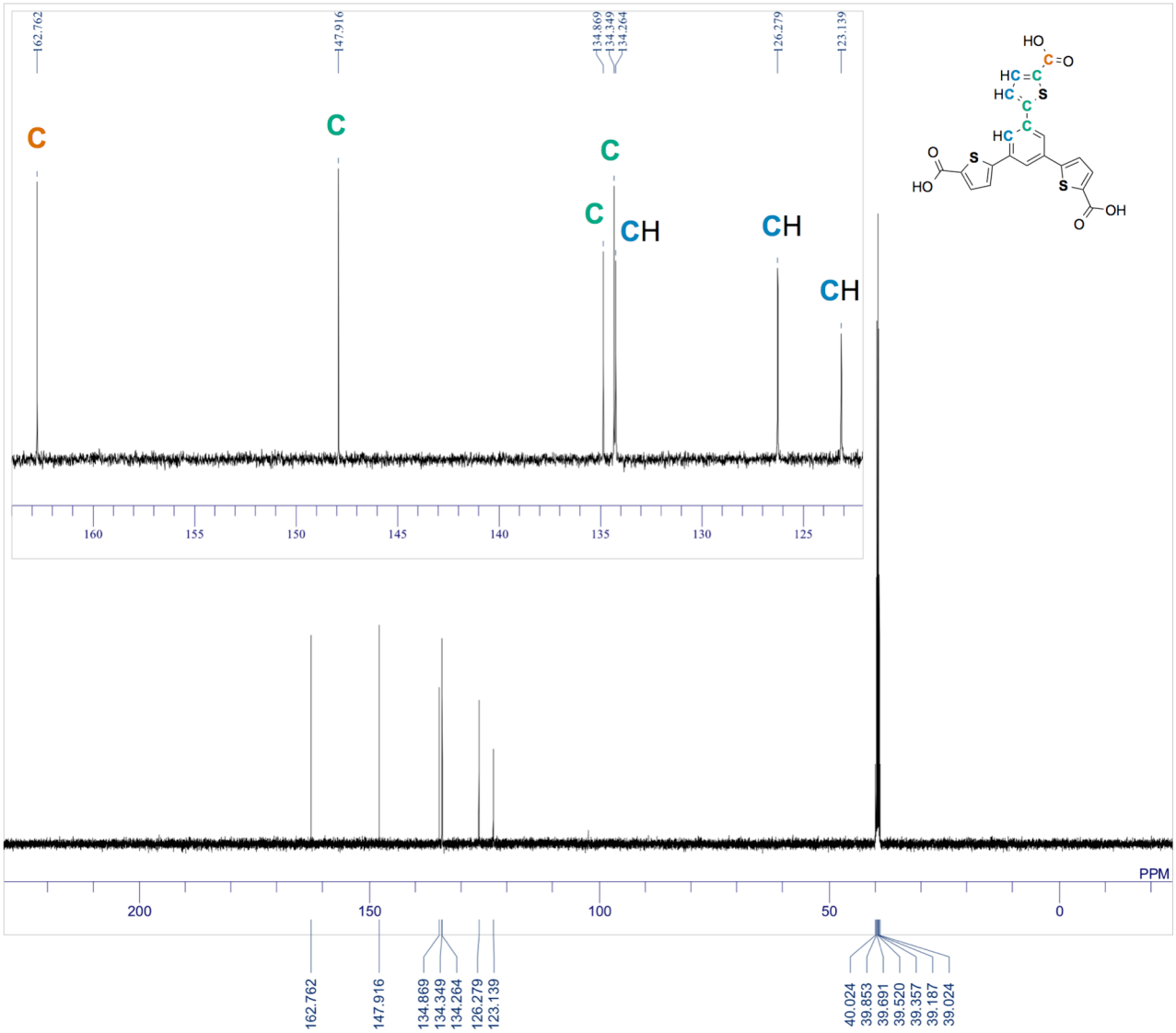

Fig. S2 ^{13}C NMR spectrum of H_3BTTc.

Synthesis of La-BTTc. (1) Powder synthesis. In a 100 mL Teflon®-lined autoclave, to the mixture of $La(NO_3)_3 \cdot 6H_2O$ (445 mg, 1.03 mmol) and H_3BTTc (468 mg, 1.03 mmol) was added DMF (50 mL). The autoclave was sealed and the mixture was stirred at 120 °C for 48 h. After cooling to room temperature, the resultant white precipitate was recovered by filtration, washed with DMF, and dried at room temperature in vacuo to afford La-BTTc including solvents in the pores (814 mg, 97% yield). Ce-, Pr-, and Nd-BTTc were also obtained by the same procedure from the corresponding $M^{III}(NO_3)_3 \cdot 6H_2O$ instead of $La(NO_3)_3 \cdot 6H_2O$. The XRPD patterns of La-, Ce-, Pr-, and Nd-BTTc are shown in Fig. S3 together with the simulated pattern of La-BTTc. The TGA trace of La-BTTc is shown in Fig. S4, from which the formula of the material is calculated as $[La(BTTc)(DMF) \cdot (DMF) \cdot 4H_2O]_\infty$.

(2) Single crystal synthesis. In a 4 mL glass vial was placed the mixture of H_3BTTc (20 μmol) and DMF solution (20 mM) of $La(NO_3)_3 \cdot 6H_2O$ (1.0 mL, 20 μmol). The vial was sealed and the mixture was placed in an oven at 120 °C for 48 h. After cooling to room temperature, a suitable crystal was mounted on a loop and analyzed to reveal its formula as $[La(BTTc)(DMF) \cdot 2(DMF)]_\infty$. Ce-BTTc was also obtained by the same procedure from $Ce(NO_3)_3 \cdot 6H_2O$ instead of $La(NO_3)_3 \cdot 6H_2O$.

The difference in the formula of the material between powder and crystal synthesis is probably due to the workup process. In powder synthesis, some DMF molecules would have been substituted by water molecules from the atmospheric moisture during the filtration and washing procedure.

X-ray Crystallographic Analysis. The intensity data were collected on a Rigaku Saturn 724+ CCD diffractometer with graphite-monochromated Mo Kα radiation (λ = 0.71070 Å). The structures were solved by a direct method (SHELXS-97)[S4] and refined by full-matrix least-squares procedures on F^2 for all reflections (SHELXL-97).[S4] The non-hydrogen atoms of the framework and the coordinated solvent ($[\underline{Ln(BTTc)(DMF)} \cdot 2(DMF)]_\infty$) were refined with anisotropic thermal parameters, while those of the free solvent ($[Ln(BTTc)(DMF) \cdot \underline{2(DMF)}]_\infty$) were refined with isotropic thermal parameters. All hydrogen atoms were placed in calculated positions. Details of the crystal data and a summary of the intensity data collection parameters for La-BTTc and Ce-BTTc are listed in Table S1. ORTEP drawings of these complexes are illustrated in Fig. S5, together with dihedral angles between the central benzene ring and the peripheral thiophene rings.

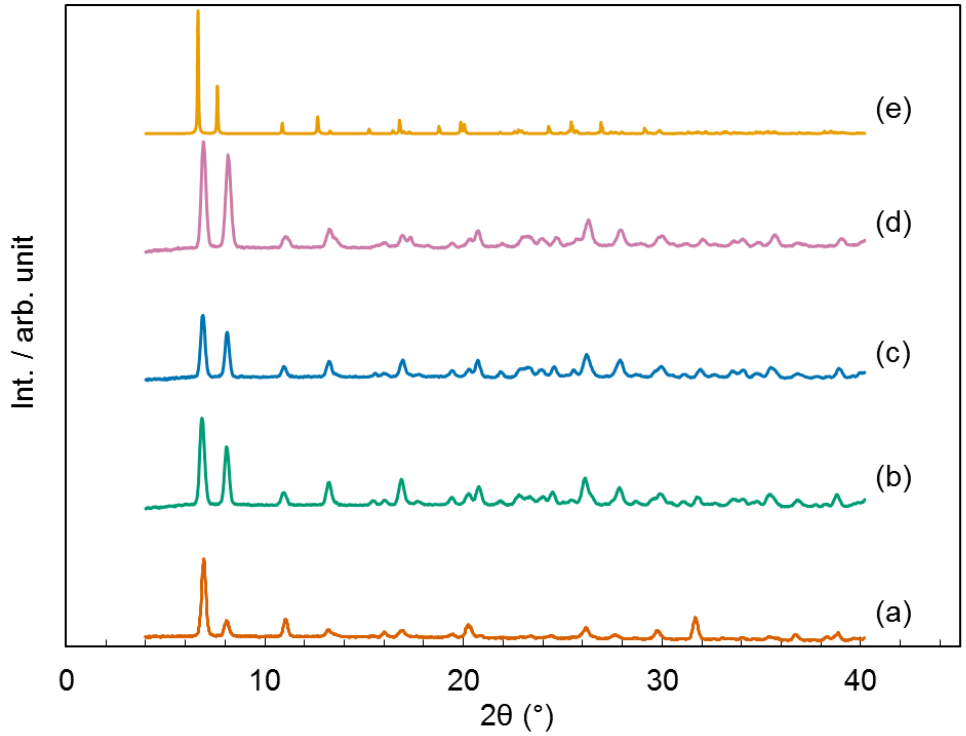

Fig. S3 The XRPD patterns of Ln-BTTc: (a) La-BTTc; (b) Ce-BTTc; (c) Pr-BTTc; (d) Nd-BTTc; (e) simulated La-BTTc.

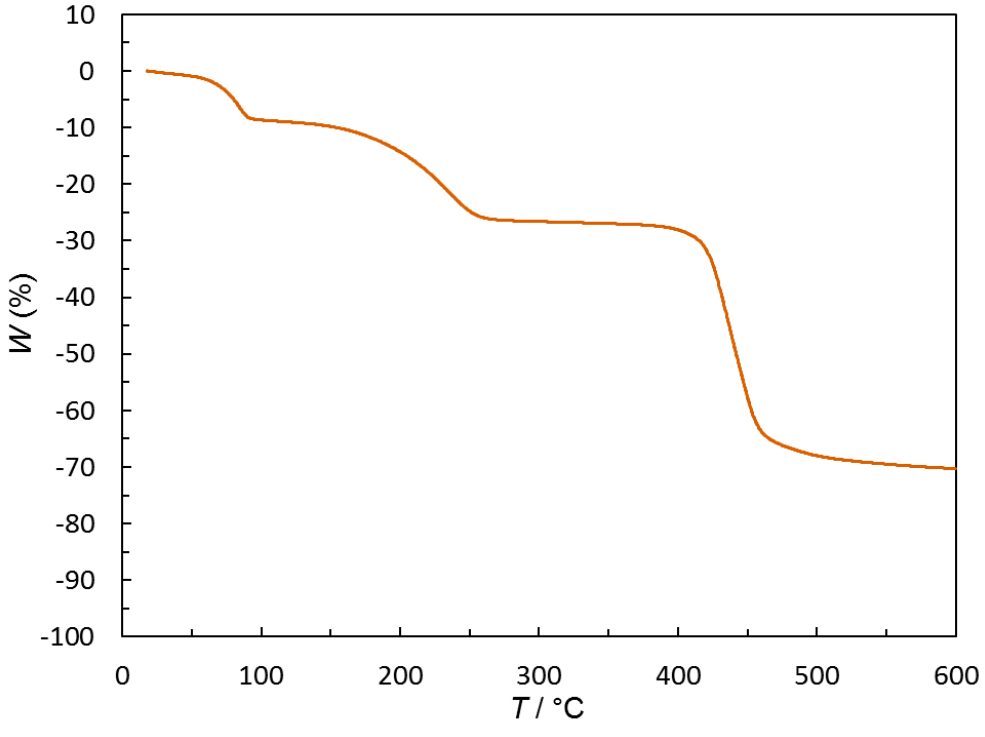

Fig. S4 TGA trace of as-synthesized La-BTTc.

Table S1 Crystallographic data and structure refinement details for La- and Ce-BTTc.

	La-BTTc	Ce-BTTc
Formula	$C_{30}H_{30}LaN_3O_9S_3$	$C_{30}H_{30}CeN_3O_9S_3$
Fw	811.66	812.87
T (K)	103(2)	103(2)
cryst system	monoclinic	monoclinic
space group	*Cc* (#9)	*Cc* (#9)
a (Å)	23.241(10)	23.293(6)
b (Å)	16.264(7)	16.237(4)
c (Å)	8.206(4)	8.172(2)
β (°)	91.544(6)	91.277(4)
V (Å^3)	3100(2)	3089.9(13)
Z	4	4
D_{calc} (g cm^{-3})	1.739	1.747
μ (mm^{-1})	1.640	1.736
F(000)	1632	1636
Flack parameter	–0.010(19)	0.03(2)
2θ range (°)	3.06–50.00	3.06–50.10
reflns collected	10373	10352
indep reflns/R_{int}	5193/0.0313	5121/0.0464
Params	372	372
completeness to θ	99.9	99.2
GOF on F^2	1.219	1.182
R_1, wR_2 ($I > 2\sigma(I)$)	0.0377, 0.1035	0.0501, 0.1359
R_1, wR_2 (all data)	0.0412, 0.1235	0.0523, 0.1448

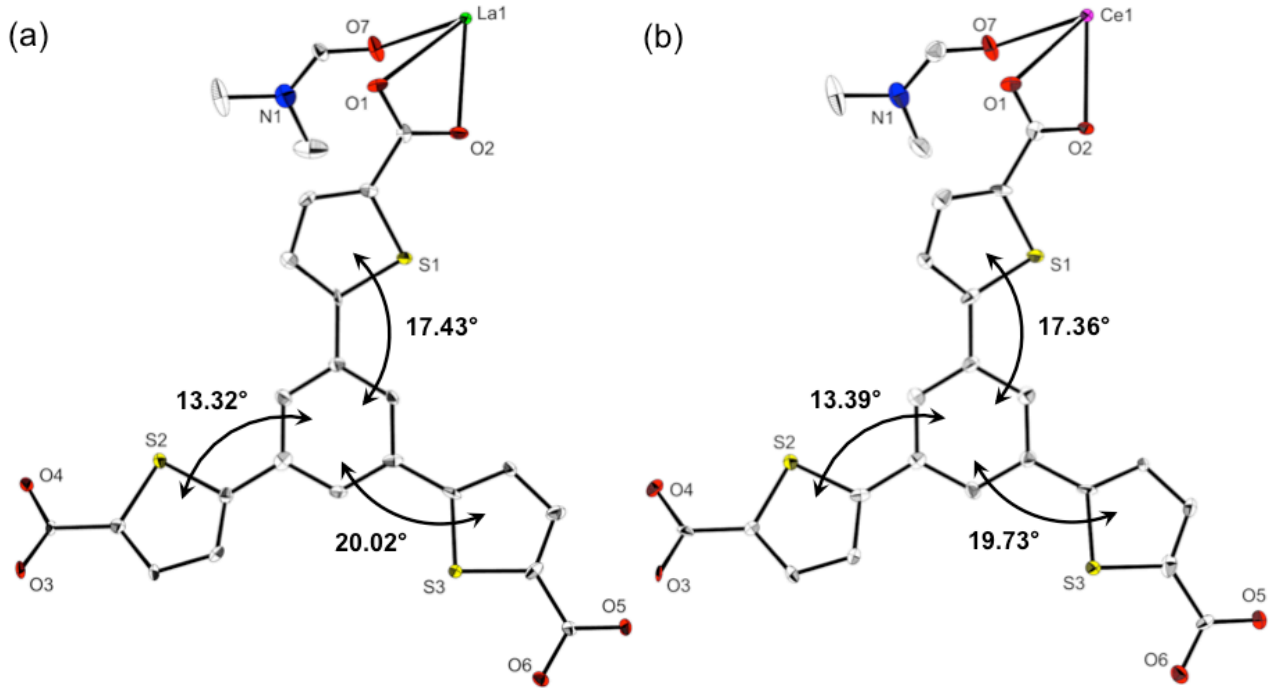

Fig. S5 ORTEP drawings of (a) La-BTTc and (b) Ce-BTTc with thermal ellipsoid plots (50% probability), showing the dihedral angles between the central benzene ring and the peripheral thiophene rings.

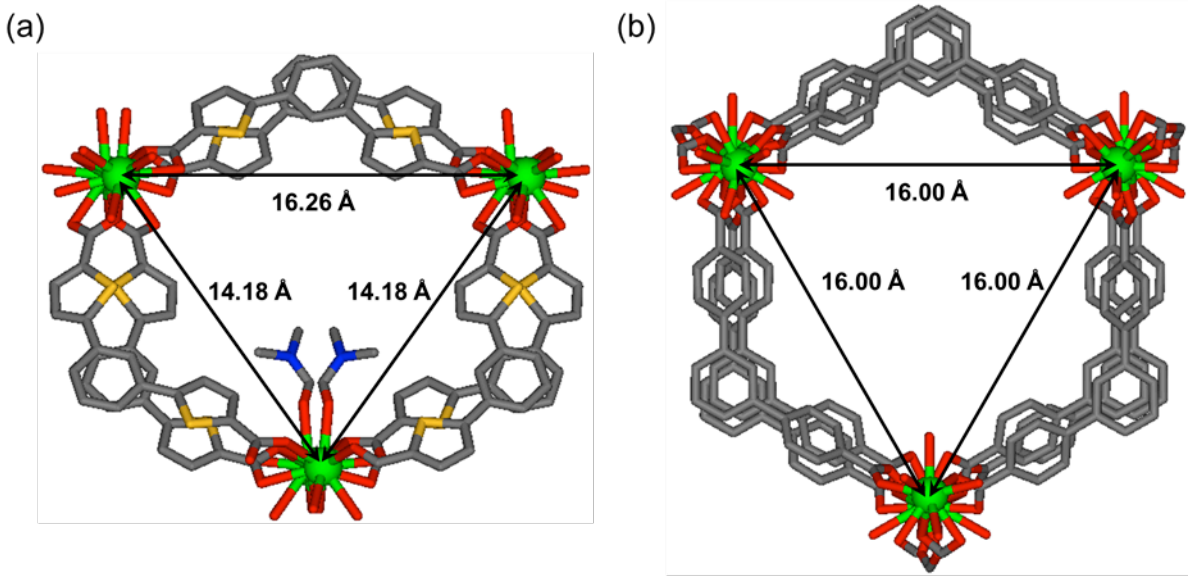

Fig. S6 One-dimensional hexagonal pores of (a) La-BTTc and (b) MIL-103(Eu) (Eu-BTB),[S2b] showing the metal–metal distances in the channel: green, metal cations; yellow, S; red, O; blue, N; gray, C.

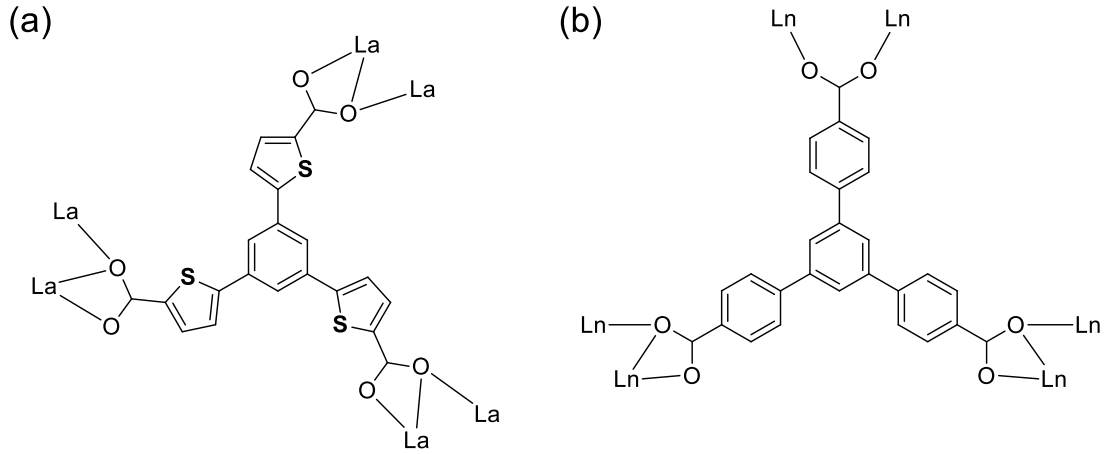

Fig. S7 Coordination modes of (a) La-BTTc and (b) MIL-103 (Ln-BTB).[S2]

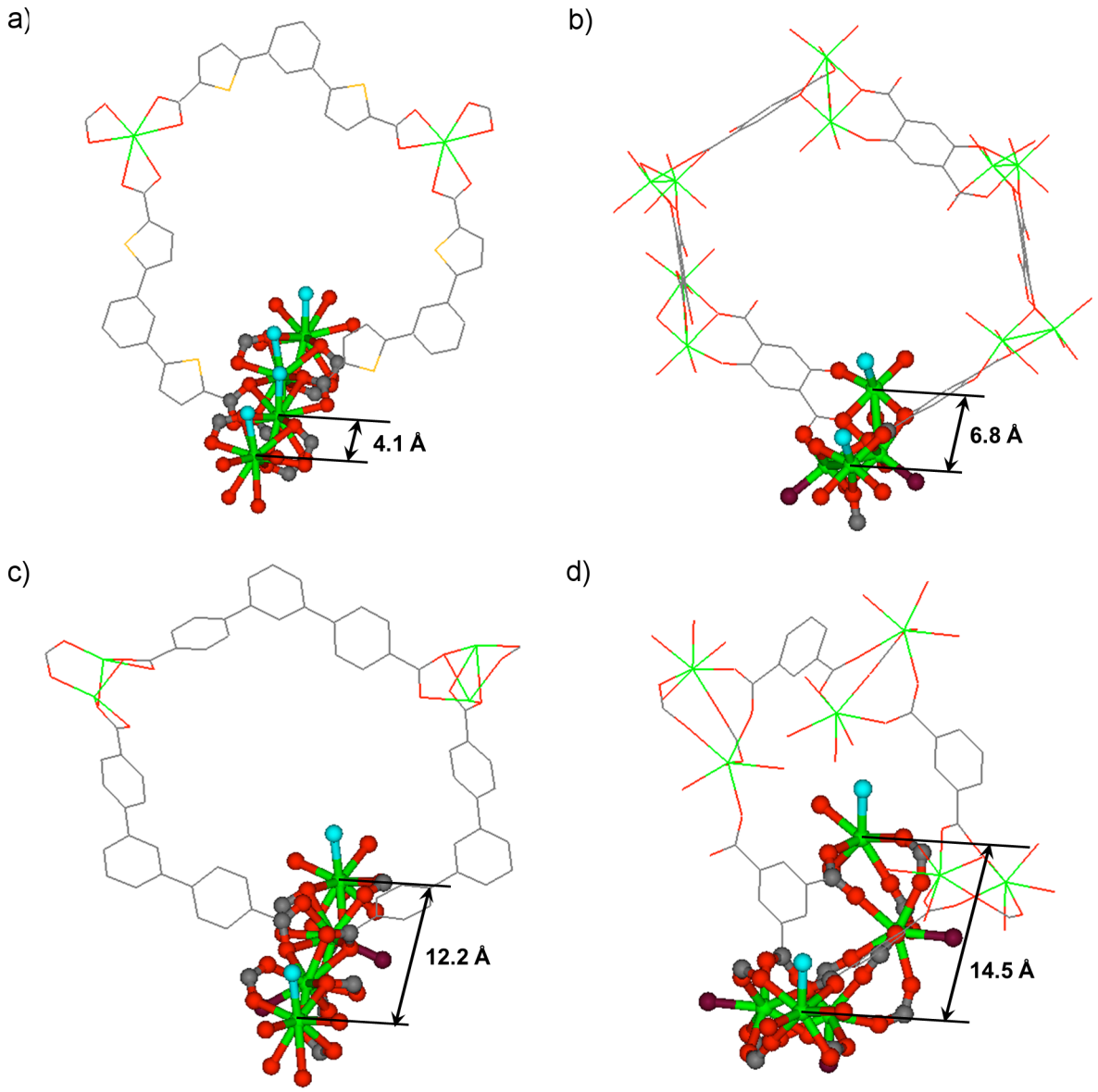

Fig. S8 One-dimensional inorganic chains in (a) La-BTTc, (b) MOF-74,[S5] (c) MIL-103,[S2] and (d) MOF-76[S6]: green, metal cations; yellow, S; red, O from carboxylate; turquoise, O from coordinated solvent which is in one pore; purple, O from coordinated solvent which is in the adjacent pores; gray, C.

Activation of La-BTTc. To a 100 mL glass vial was added La-BTTc (810 mg) and EtOH (55 mL). The vial was capped and the mixture was allowed to stand at room temperature for 72 h, during which time the solvent was exchanged twice by the removal of the supernatant and the addition of fresh EtOH. Filtration and washing with EtOH afforded the EtOH-exchanged La-BTTc (692 mg). The TGA trace is shown in Fig. S9. The EtOH-exchanged samples were heated at 200 °C for 6 h in vacuo to give the activated La-BTTc. The XRPD patterns of La-BTTc during the activation steps are shown in Fig. S10. Nitrogen isotherm of the activated La-BTTc is shown in Fig. S11.

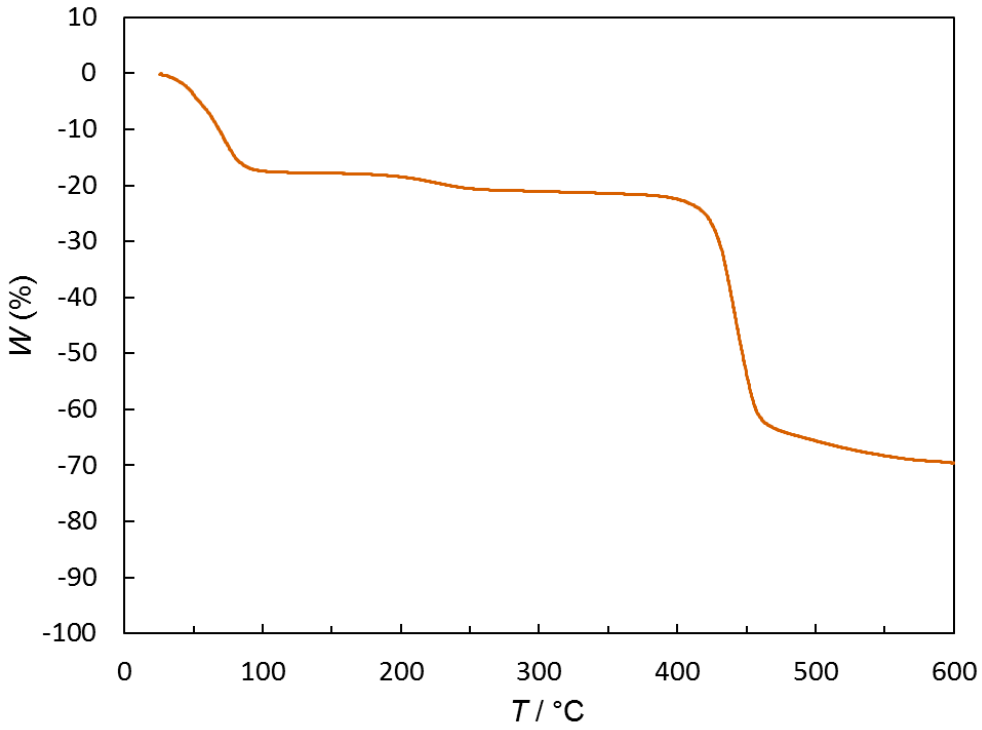

Fig. S9 TGA trace of La-BTTc after soaking in EtOH.

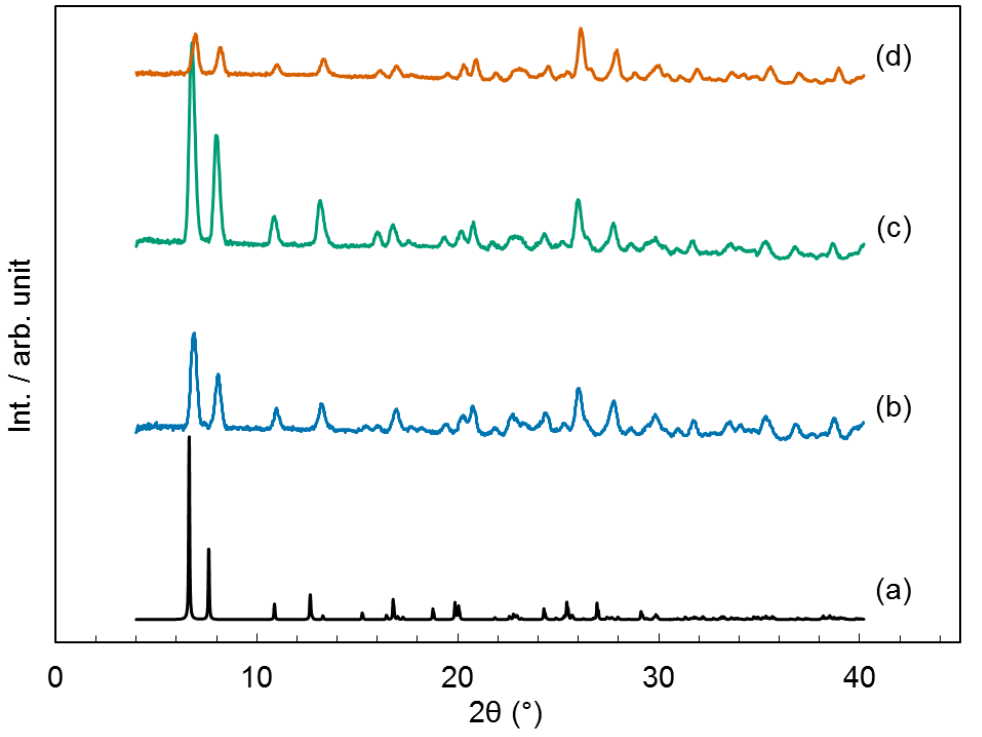

Fig. S10 The XRPD patterns of La-BTTc: (a) simulated; (b) as-synthesized; (c) after soaking in ethanol; (d) after heating at 200 °C in vacuo.

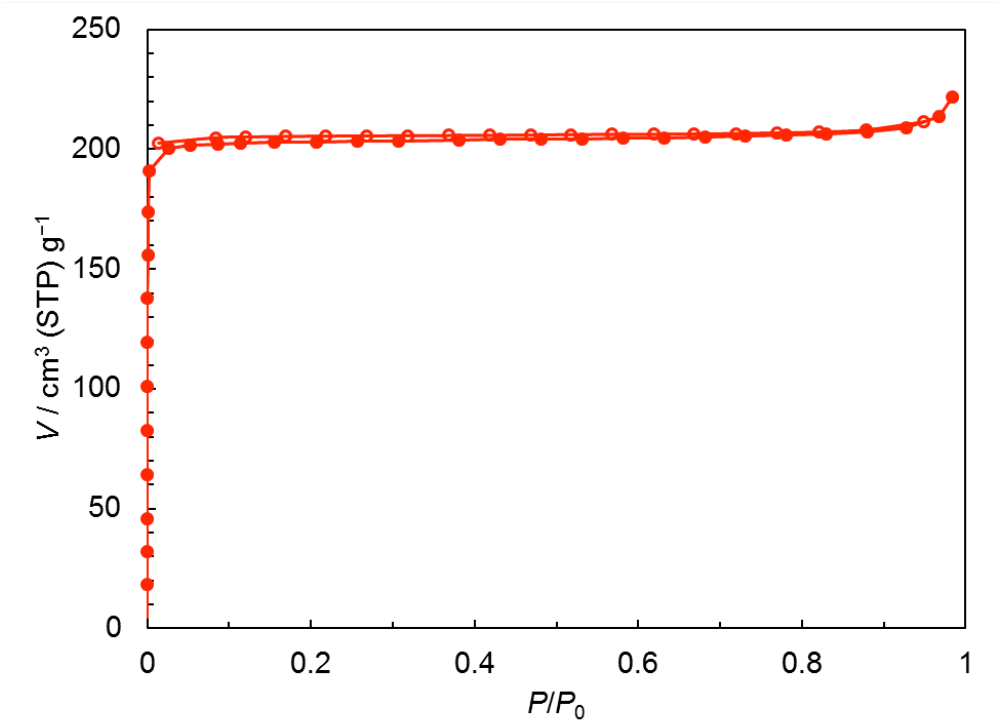

Fig. S11 Nitrogen isotherms of La-BTTc at 77 K: ●, adsorption; ○, desorption.

IR Spectra of Acetone-adsorbed PCPs. Acetone-adsorbed PCPs were prepared by the following procedure. Small amounts (5–10 mg each) of activated samples of PCPs were weighed in 8 mm ø microtubes as quickly as possible to prevent adsorption of water from air. The microtubes were placed in a Schlenk flask, and the flask was heated with an oil bath at 100 °C under dynamic vacuum for 2 h. After the flask was cooled to room temperature, dry acetone (0.5 mL) was added via syringe to the bottom of the flask under static vacuum. The flask was allowed to stand at room temperature under static vacuum for 1 h, during which time acetone was vaporized and adsorbed inside the micropores of PCPs. The samples of acetone-adsorbed PCPs in the microtubes were taken out of the flask, and the IR spectra were recorded using the attenuated total reflectance (ATR) method. The IR spectra are shown in Fig. S12–S15.

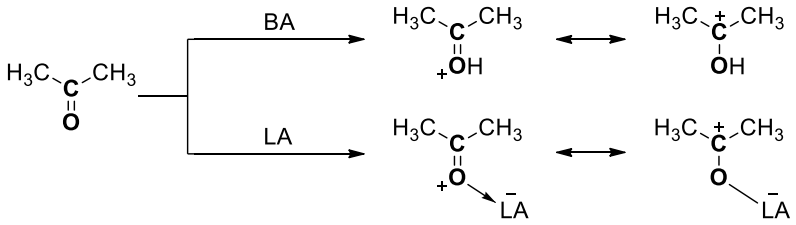

Scheme S2 Interaction of acetone with acidic sites.

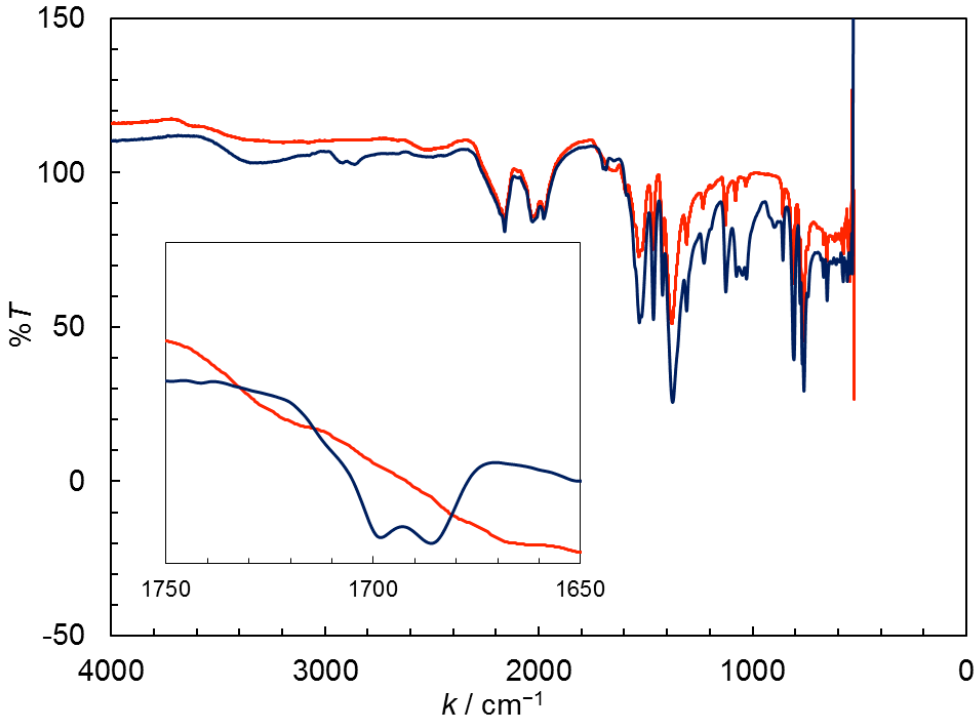

Fig. S12 IR spectra of activated (red) and acetone-adsorbed (blue) La-BTTc.

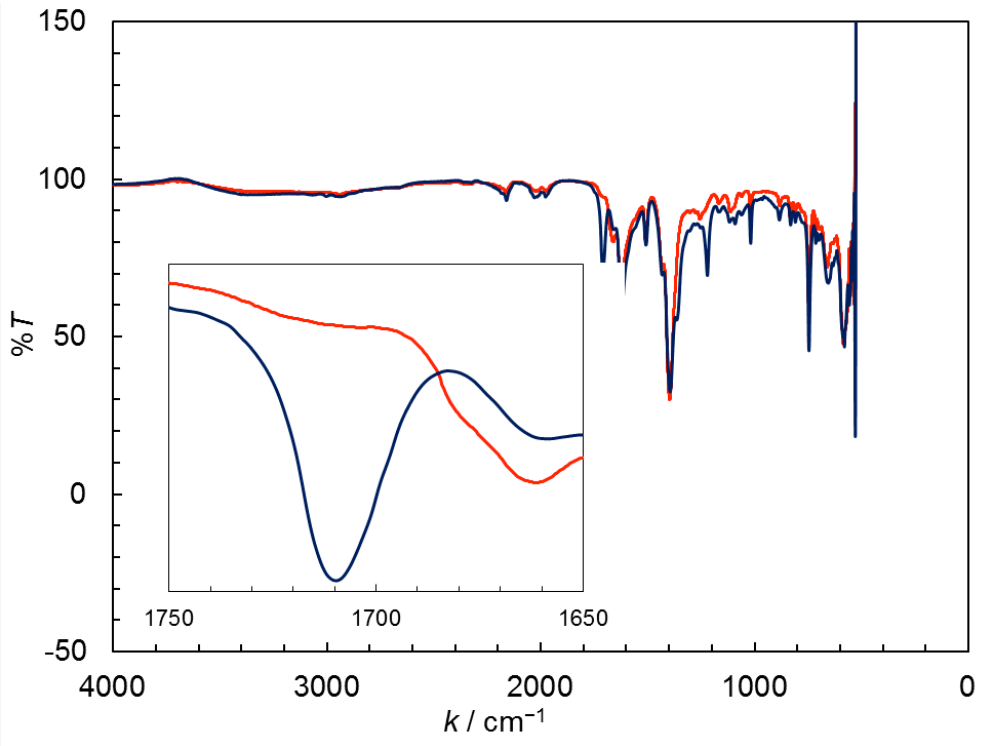

Fig. S13 IR spectra of activated (red) and acetone-adsorbed (blue) MIL-101(Cr).

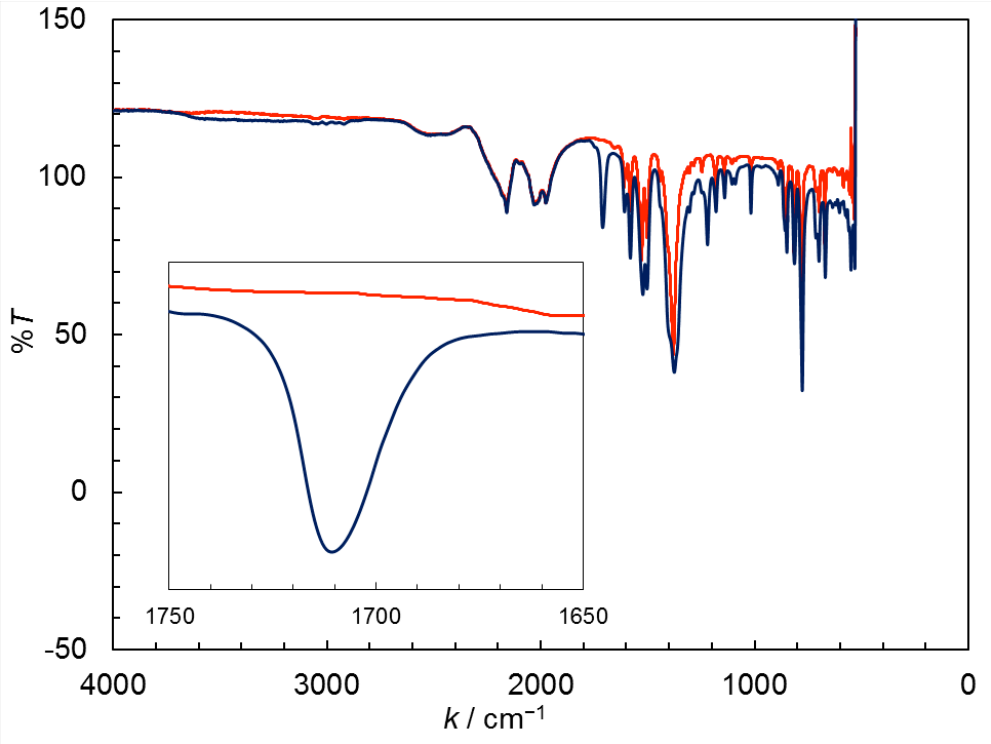

Fig. S14 IR spectra of activated (red) and acetone-adsorbed (blue) MIL-103(La).

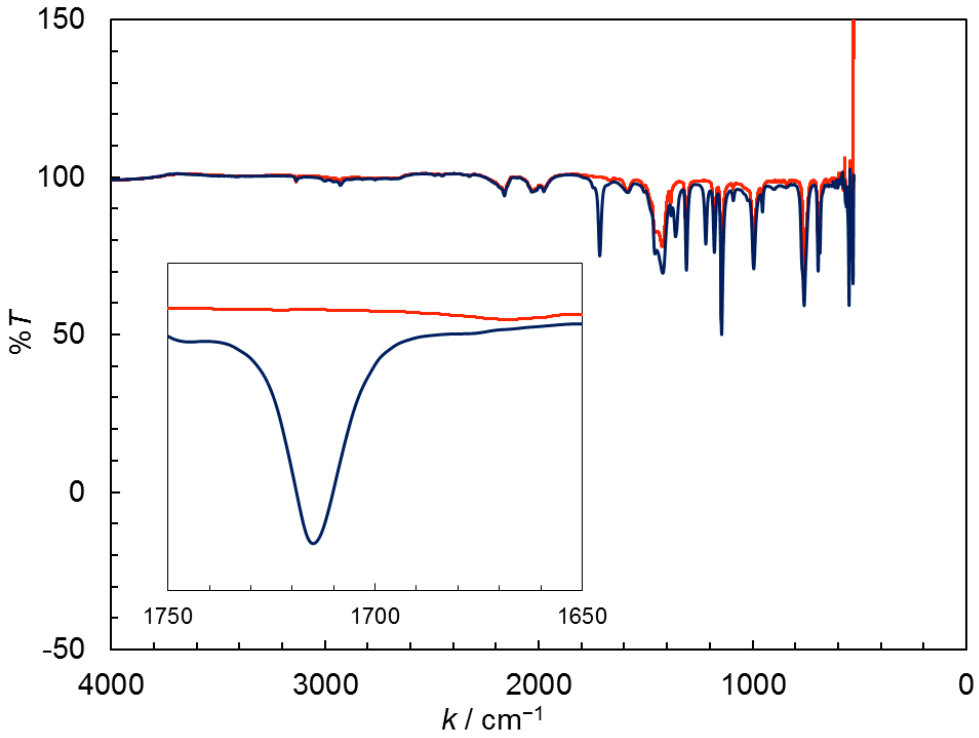

Fig. S15 IR spectra of activated (red) and acetone-adsorbed (blue) ZIF-8.

Discussion on the IR Spectra. As seen in Fig. S12, two bands were observed in the region of the carbonyl stretching vibration for acetone-adsorbed La-BTTc. This phenomenon indicates that there are two kinds of acetone molecules interacting with acidic sites. One possible explanation is that due to the steric hindrance, acetone cannot coordinate strongly to the La cation after the next OMS is occupied with another acetone molecule (Fig. S16a). This is in agreement with the short distance of the neighboring OMSs in La-BTTc (4.1 Å) and the kinetic diameter of acetone (4.6 Å).[S7] Another possibility is that some of LA sites in La-BTTc are blocked by the residual water molecules and acetone is interacted with both LA sites of La cation and BA sites of coordinated water (Fig. S16b). Similar Brønsted acidity has been reported in the LA sites of MIL-100(Cr).[S8] When the sample was allowed to stand under humid air for 1 h before adsorption of acetone, it showed only one peak at 1690.8 cm^{-1}, different from both two of the activated sample (Table 1 in the main text). Because this new peak seems to result from the induced BA sites of the adsorbed water molecules, the observation of two peaks for the activated sample is plausibly due to the mechanism (a).

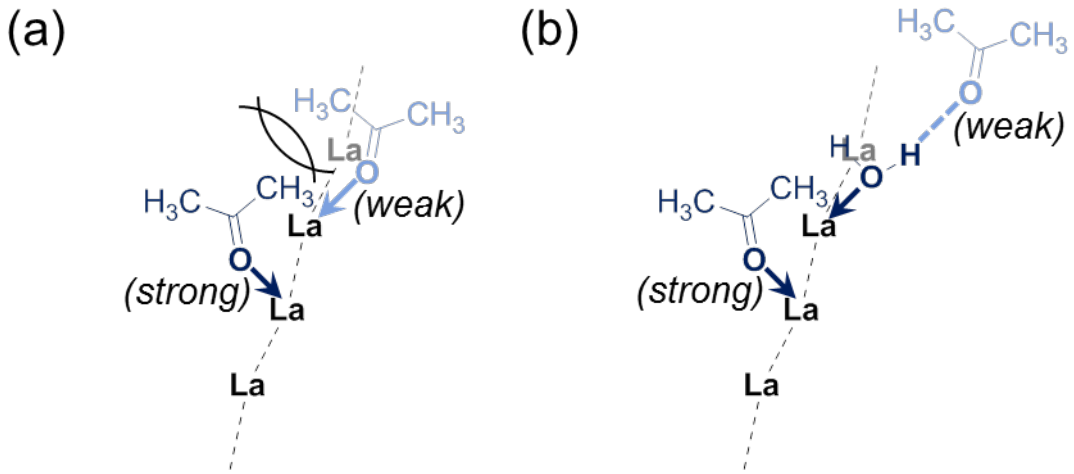

Fig. S16 Possible mechanisms for the observation of two carbonyl stretching vibrations: (a) steric repulsion between the neighboring acetone molecules; (b) interaction with LA sites of La cation and induced BA sites of the residual water molecules.

Stability of La-BTTc toward NH_3. Stability test was conducted by the following procedure. Small amounts (10–15 mg each) of degassed samples of PCPs were weighed in 8 mm ø microtubes as quickly as possible to prevent adsorption of water from air. The microtubes were placed in a Schlenk flask, and the flask was heated with a mantle heater at 100 °C under dynamic vacuum for 2 h. After the flask was cooled to room temperature, ammonia was introduced into the flask until the pressure in the flask became 1 atm. Ammonia was kept flowing at a slow rate while the flask was heated with a mantle heater to a desired temperature, held at the temperature for 2 h, cooled to room temperature. Then the samples were purged at room temperature for 2 h in flowing nitrogen. The samples of PCPs in the microtubes were taken out of the flask, and their framework structures were investigated with XRPD. Stability of the samples was evaluated by comparing the XRPD patterns with those of degassed samples.

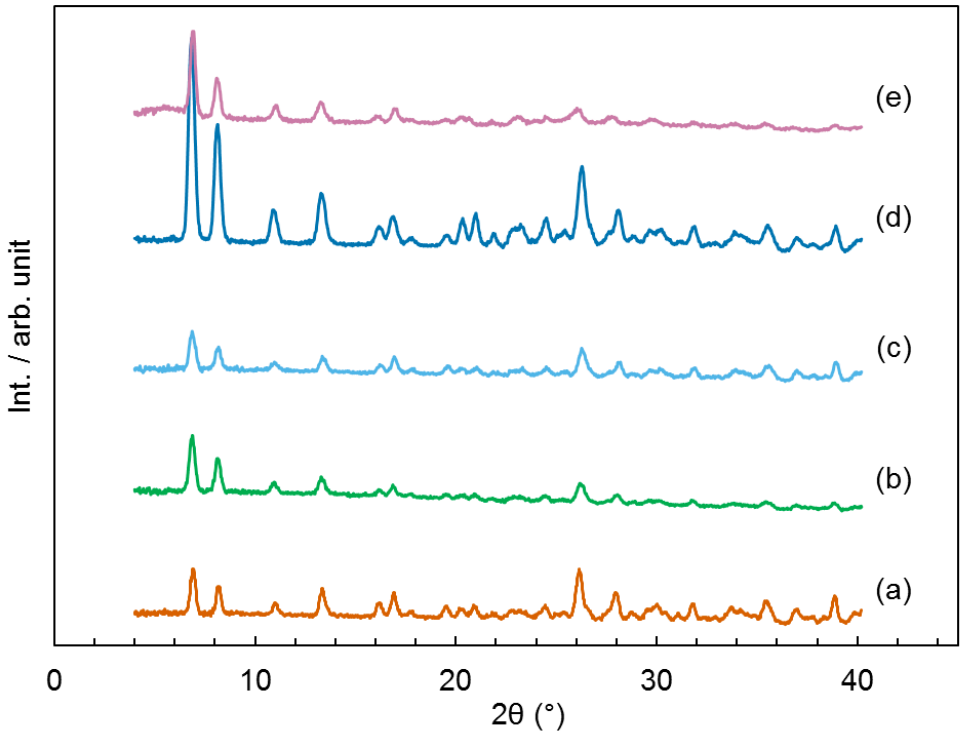

Fig. S17 The XRPD patterns of La-BTTc: (a) before exposure to NH_3; after exposure to NH_3 (b) at room temperature, (c) at 200 °C, (d) at 300 °C, and (e) at 350 °C.

Discussion on the NH_3-TPD. The TPD data were collected using a heating rate of 5 K min^{-1} under He (30 mL min^{-1}) with Q-mass (m/z = 16) as a detector.

In Table S2 are summarized the peak temperature and the observed and calculated acid density. In La-BTTc, the largest desorption peak was observed at a very high temperature of 480 °C, followed by a shoulder at 500 °C and a small additional peak at 550 °C (Table S2). It should be noted that these values are above the decomposition temperature of La-BTTc estimated from the TGA (ca. 430 °C, Figs. S4 and S9). Therefore, the exact acid strength of La-BTTc cannot be evaluated. The proper peak value is assumed to be greater than or equal to 430 °C. This value is still much higher than that reported for MIL-101(Cr)[S9] and that observed for H-ZSM-5 (Table S2). From the NH_3-TPD measurement, the order of the acid strength is La-BTTc > H-ZSM-5 > MIL-101(Cr). The stronger acidity of La-BTTc compared to MIL-101(Cr) is also observed in the IR spectroscopy using acetone as a probe (see the main text).

Table S2 Peak temperature of NH_3 desorption and acid density of PCP and zeolite.

porous material	T_{des} [a]/°C	D_{obsd} [b]/mmol g^{-1}	D_{calcd} [c]/mmol g^{-1}
La-BTTc	480, 500, (550)	1.39	1.69
MIL-101(Cr)	260[d]	2.91[d]	2.94[d]
H-ZSM-5[e]	170, 330, (510)	0.34	0.33

[a] Peak temperature of NH_3 desorption. Small additional peaks are shown in the parentheses. [b] Observed acid density. [c] Calculated acid density from their molecular formula. [d] ref. S9. [e] The SiO_2/Al_2O_3 ratio is 100.

Discussion on the Origin of the Strong Acidity of La-BTTc. In the case of MIL-103 (Ln-BTB), the removal of the coordinated solvent is accompanied with the change in coordination mode of one μ-carboxylato-1κ*O*:2κ*O′* carboxylate group to μ-carboxylato-1κ^2*O*:2κ*O* mode, which maintains the coordination geometry around the metal center (*TPRS*-9, Fig. S18a).[S2b] By contrast, the removal of DMF cannot result in any changes in coordination mode of the linker in La-BTTc because all carboxylate groups adopt μ-carboxylato-1κthe ^{2}*O*:2κ*O* fashion in the as-synthesized state. Thus, the activation of La-BTTc would lead to a highly distorted nine-coordinated metal center and would show strong acidity (Fig. S18b).

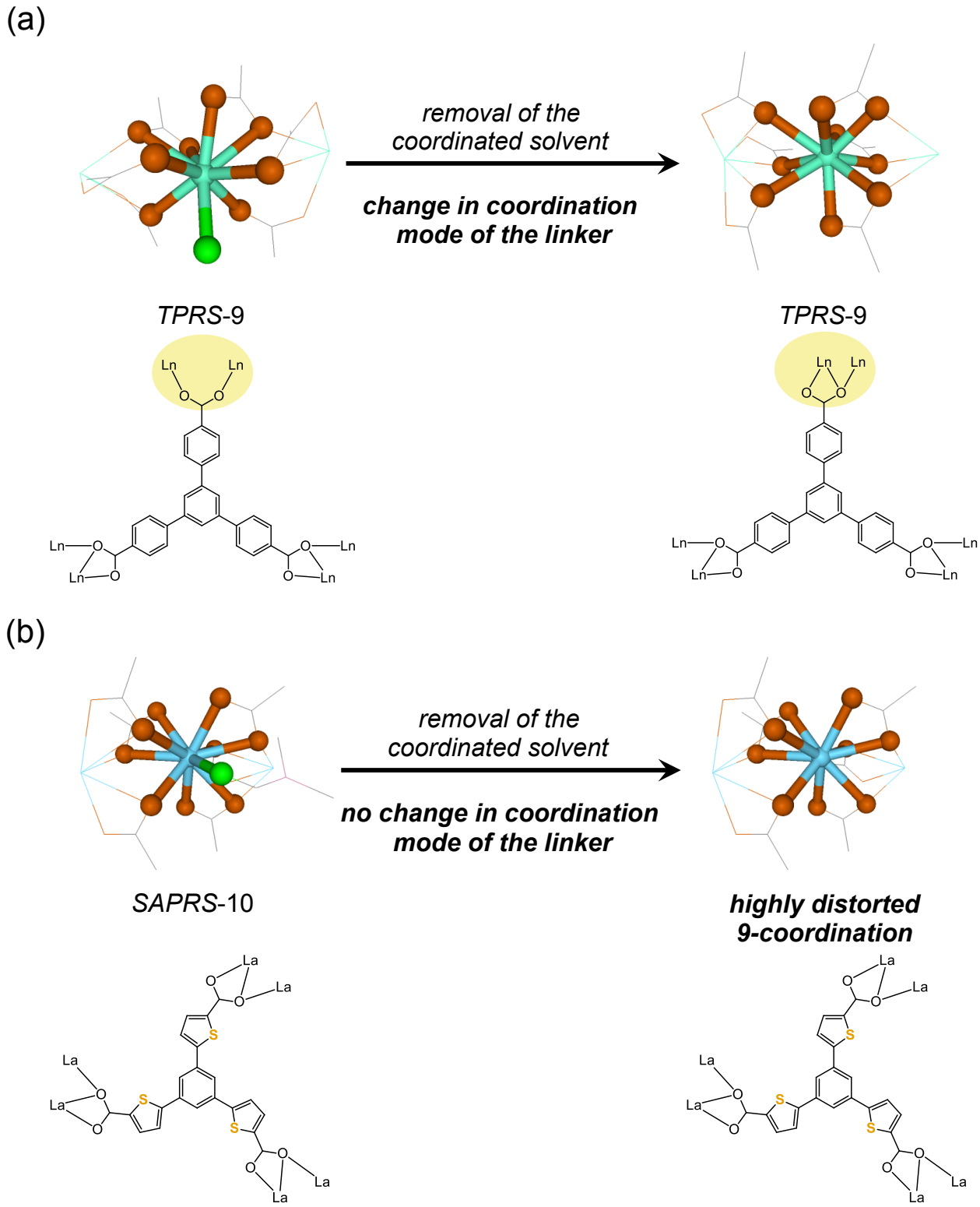

Fig. S18 (a) Change in coordination mode of the linker in MIL-103 (Ln-BTB) during its activation step, which is reported in ref. S2b; (b) possible explanation on the origin of the strong acidity of La-BTTc.

Cyanosilylation Reactions of Benzaldehyde. The activated La-BTTc was weighed in a glass vial as quickly as possible to prevent adsorption of water from air. The vial was heated at 200 °C under dynamic vacuum for 2 h. After the vial was cooled to room temperature, benzaldehyde (PhCHO) and trimethylsilyl cyanide (TMSCN) were added under N_2. The mixture was stirred at room temperature for several hours (t_1). After filtration, the aliquot of the liquid was dissolved in $CDCl_3$ and the ^1H NMR spectrum was recorded to evaluate the progress of the reaction. To confirm the heterogeneity of the reaction, the liquid after the filtration was further stirred at room temperature for additional hours (t_2) and analyzed again. The results are summarized in Table S3.

Table S3 Results of cyanosilylation reactions of benzaldehyde in the presence of La-BTTc.[a]

entry	La-BTTc /mmol[b,c]	PhCHO /mmol	TMSCN /mmol	t_1/h[d]	yield (%)[e]	t_2/h[f]	yield (%)[e]
1	0.05 (10)	0.5	1.0	1	>99	—	—
2	0.04 (1)	4.0	4.0	0.5	68	1.5	66
3	0.04 (1)	4.0	4.0	1	71	19	72
4	0.04 (1)	4.0	4.0	2	82	1	82

[a] At r.t. under N_2. [b] Calcd from its molecular formula (1.69 mmol g^{-1} for $[La(BTTc)]_\infty$). [c] mol % to PhCHO is shown in the parentheses. [d] Time of the catalytic reaction. [e] Determined by the ratio of the integrated intensities of the formyl proton of PhCHO (10.03 ppm) and the methine proton of the product (5.50 ppm). [f] Time of the additional stirring after the filtration.

Discussion on the Catalytic Activity. To compare the catalytic activity of La-BTTc with those of known PCPs, the reported results are summarized in Table S4. Because the reaction conditions are different in each literature, the comparison of the yields is not appropriate. Therefore, we have calculated the TON and TOF values for the comparison. The large TON and TOF values calculated for La-BTTc strongly indicate the high activity of this material. It should be noted that our reaction conditions are milder than those reported in the literatures (smaller amounts of TMSCN and lower temperature).

Table S4 Comparison of the catalytic activity of PCPs in cyanosilylation reactions of benzaldehyde.

catalyst	mol % cat	molar ratio[a]	solvent	*T* /°C	*t* /h	yield (%)	TON[b]	TOF[c] /h^{-1}	ref
La-BTTc	1	1:1	neat	r.t.	0.5	68	68	136	this work
La-BTTc	1	1:1	neat	r.t.	2	82	82	41	this work
MIL-101(Cr)	1	1:2	heptane	40	3	98	98	33	S10
RPF-21-La	1	1:1.5	neat	40	4	93	93	23	S11
$[Zn_2(ptaH)_2]_\infty$	1	1:2	CH_2Cl_2	0	2	32	32	16	S12
$[Nd(btc)]_\infty$	4.5	1:2	CH_2Cl_2	r.t.	2	99	22	11	S6c
$[Nd(btc)]_\infty$	9	1:2	neat	r.t.	1	88	9.8	9.8	S6c
$[Fe_2Ag_2(pca)_4(pcaH)_4(ClO_4)_2]_\infty$	1.7	1:2	CH_2Cl_2	r.t.	3	51	30	10	S13
RPF-19-Nd	5	1:1.5	neat	50	2	95	19	9.5	S14
RPF-18-La	5	1:1.5	neat	50	2	86	17	8.6	S14
Ce-MDIP1	2	1:2.4	CH_3CN	r.t.	11	100	50	4.5	S15
$[Sc_2(C_4O_4)_3]_\infty$	2	1:2	CH_2Cl_2	40	12	90	45	3.8	S16
$[Zn_3(TCPB)_2]_\infty$	2.5	1:2	hexane	r.t.	13	100	40	3.1	S17
(O_2H_3)Sc-MOF	5	1:1.5	neat	40	8	84	17	2.1	S18
$[Mn_3\{(Mn_4Cl)_3(BTT)_8\}_2]_\infty$	11	1:2	CH_2Cl_2	r.t.	9	98	8.9	0.99	S19
$[Co_{0.5}Ni_{0.5}(Bpe)(VO_3)_2]_\infty$	10	1:5	neat	50	16	77	7.7	0.48	S20
$[Sm(L\text{-}H_3)(L\text{-}H_2)]_\infty$	11	1:2	CH_2Cl_2	r.t.	16	69	6.3	0.39	S21
$[Cd(bpy)_2(NO_3)_2]_\infty$	20	1:2	CH_2Cl_2	40	24	77	3.8	0.16	S22
$[Cu_3(BTC)_2]_\infty$	16	1:2	heptane	60	48	55	3.4	0.07	S23
$[Zn_3(bpy)_{3.5}(\mu\text{-}O_2CH)_4(ClO_4)_2]_\infty$	13	1:2	CH_2Cl_2	r.t.	24	22	1.7	0.07	S24

[a] PhCHO:TMSCN. [b] TON = (yield)/(mol % cat). [c] TOF = (TON)/(*t*).

Reaction of 1-Hexene. The reaction of 1-hexene was conducted by utilizing the apparatus shown in Fig. S19. The sample was loaded in a glass insert [b] and activated at 200 °C for 30 min under a flow of He. After heating to the reaction temperature shown in Table S5, the stop valves [e] were closed and 1-hexene was added via INJ-1. 1-Hexene was allowed to react in the closed reaction system for 7 min. Then the six port valve [a] was switched to the dashed lines. The reaction mixture was analyzed by the GC using capillary [c] and packed columns [d] with FID as a detector. The product distribution is summarized in Table S5. In Fig. S20 are shown the XRPD patterns of La-BTTc after the reaction, which is almost unchanged compared with the sample before the reaction.

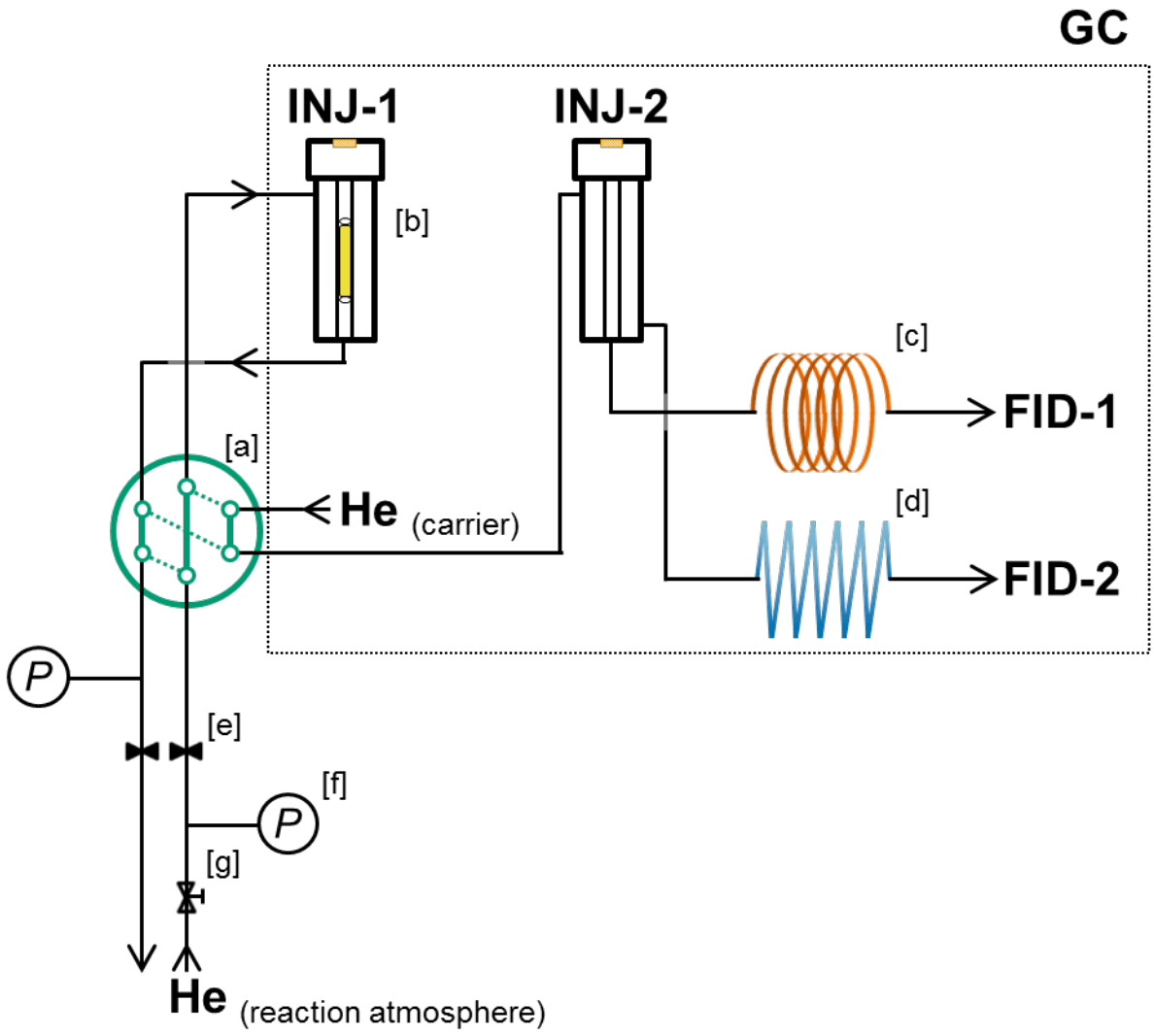

Fig. S19 Schematic representation of the apparatus for the reaction of 1-hexene: [a] six port valve; [b] catalyst loaded inside a glass insert; [c] capillary column; [d] packed column; [e] stop valve; [f] pressure gauge; [g] pressure control valve.

Table S5 Distribution of the reaction mixture of 1-hexene for 7 min under He.

product	300 °C		350 °C		400 °C	
	none	La-BTTc	none	La-BTTc	none	La-BTTc
cracking products (C_{1-5} hydrocarbon)	0.13	0.12	0.14	0.57	0.86	2.42
isomerization products (C_6 hydrocarbon)	3.14	1.83	4.32	4.65	25.60	21.61
unreacted substrate (1-hexene)	96.47	97.99	93.95	94.36	73.04	73.73
other products (C_{7+} and aromatics)	0.27	0.06	1.58	0.42	0.51	2.24

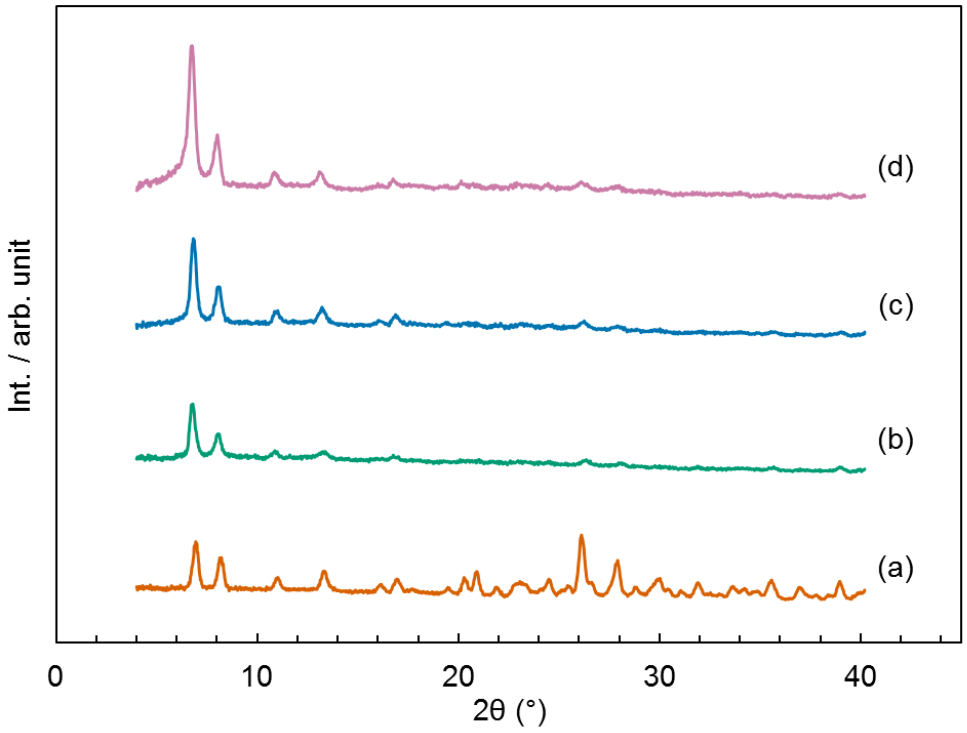

Fig. S20 The XRPD patterns of La-BTTc: (a) before the reaction; after the reaction of 1-hexene (b) at 300 °C, (c) at 350 °C, and (d) at 400 °C for 7 min.

References

S1 (*a*) G. Férey, C. Mellot-Draznieks, C. Serre, F. Millange, J. Dutour, S. Surblé and I. Margiolaki, *Science* 2005, **309**, 2040–2042; (*b*) N. A. Khan, I. J. Kang, H. Y. Seok and S. H. Jhung, *Chem. Eng. J.* 2011, **166**, 1152–1157; (*c*) E. Haque, N. A. Khan, J. E. Lee and S. H. Jhung, *Chem. Eur. J.* 2009, **15**, 11730–11736.

S2 (*a*) T. Devic, C. Serre, N. Audebrand, J. Marrot and G. Férey, *J. Am. Chem. Soc.* 2005, **127**, 12788–12789; (*b*) T. Devic, V. Wagner, N. Guillou, A. Vimont, M. Haouas, M. Pascolini, C. Serre, J. Marrot, M. Daturi, F. Taulelle and G. Férey, *Microporous Mesoporous Mater.* 2011, **140**, 25–33.

S3 (*a*) X.-C. Huang, Y.-Y. Lin, J.-P. Zhang and X.-M. Chen, *Angew. Chem. Int. Ed.* 2006, **45**, 1557–1559; (*b*) K. S. Park, Z. Ni, A. P. Côté, J. Y. Choi, R. Huang, F. J. Uribe-Romo, H. K. Chae, M. O'Keeffe and O. M. Yaghi, *Proc. Natl.Acad. Sci. U.S.A.* 2006, **103**, 10186–10191.

S4 G. M. Sheldrick, *Acta Crystallogr., Sect. A: Found. Crystallogr.* 2008, **64**, 112–122.

S5 (*a*) N. L. Rosi, J. Kim, M. Eddaoudi, B. Chen, M. O'Keeffe and O. M. Yaghi, *J. Am. Chem. Soc.* 2005, **127**, 1504–1518; (*b*) P. D. C. Dietzel, Y. Morita, R. Blom and H. Fjellvåg, *Angew. Chem. Int. Ed.* 2005, **44**, 6354–6358; (*c*) P. D. C. Dietzel, B. Panella, M. Hirscher, R. Blom and H. Fjellvåg, *Chem. Commun.* 2006, 959–961.

S6 (*a*) X. Guo, G. Zhu, Z. Li, F. Sun, Z. Yang and S. Qiu, *Chem. Commun.* 2006, 3172–3174; (*b*) H.-L. Jiang, N. Tsumori and Q. Xu, *Inorg. Chem.* 2010, **49**, 10001–10006; (*c*) M. Gustafsson, A. Bartoszewicz, B. Martín-Matute, J. Sun, J. Grins, T. Zhao, Z. Li, G. Zhu and X. Zou, *Chem. Mater.* 2010, **22**, 3316–3322.

S7 L. Gales, A. Mendes, C. Costa, *Carbon* 2000, **38**, 1083–1088.

S8 A. Vimont, J.-M. Goupil, J.-C. Lavalley, M. Daturi, S. Surblé, C. Serre, F. Millange, G. Férey, N. Audebrand, *J. Am. Chem. Soc.* 2006, **128**, 3218–3227.

S9 Y. Pan, B. Yuan, Y. Li, D. He, *Chem. Commun.* 2010, **46**, 2280–2282.

S10 A. Henschel, K. Gedrich, R. Kraehnert and S. Kaskel, *Chem. Commun.* 2008, 4192–4194.

S11 R. F. D'Vries, V. A. de la Peña-O'Shea, N. Snejko, M. Iglesias, E. Gutiérrez-Puebla and M. A. Monge, *Cryst. Growth Des.* 2012, **12**, 5535–5545.

S12 S. Neogi, M. K. Sharma and P. K. Bharadwaj, *J. Mol. Catal. A: Chem.* 2009, **299**, 1–4.

S13 S. Nayak, K. Harms and S. Dehnen, *Inorg. Chem.* 2011, **50**, 2714–2716.

S14 R. F. D'Vries, M. Iglesias, N. Snejko, E. Gutiérrez-Puebla and M. A. Monge, *Inorg. Chem.* 2012, **51**, 11349–11355.

S15 D. Dang, P. Wu, C. He, Z. Xie and C. Duan, *J. Am. Chem. Soc.* 2010, **132**, 14321–14323.

S16 F. Gándara, B. Gómez-Lor, M. Iglesias, N. Snejko, E. Gutiérrez-Puebla and A. Monge, *Chem. Commun.* 2009, 2393–2395.

S17 X.-M. Lin, T.-T. Li, Y.-W. Wang, L. Zhang and C.-Y. Su, *Chem. Asian J.* 2012, **7**, 2796–2804.

S18 R. F. D'Vries, V. A. de la Peña-O'Shea, N. Snejko, M. Iglesias, E. Gutiérrez-Puebla and M. A. Monge, *J. Am. Chem. Soc.* 2013, **135**, 5782–5792.

S19 S. Horike, M. Dincă, K. Tamaki and J. R. Long, *J. Am. Chem. Soc.* 2008, **130**, 5854–5855.

S20 R. Fernández de Luis, M. K. Urtiaga, J. L. Mesa, E. S. Larrea, M. Iglesias, T. Rojo and M. I. Arriortua, *Inorg. Chem.* 2013, **52**, 2615–2626.

S21 O. R. Evans, H. L. Ngo and W. Lin, *J. Am. Chem. Soc.* 2001, **123**, 10395–10396.

S22 M. Fujita, Y. J. Kwon, S. Washizu and K. Ogura, *J. Am. Chem. Soc.* 1994, **116**, 1151–1152.

S23 K. Schlichte, T. Kratzke and S. Kaskel, *Microporous Mesoporous Mater.* 2004, **73**, 81–88.

S24 P. Phuengphai, S. Youngme, P. Gamez and J. Reedijk, *Dalton Trans.* 2010, **39**, 7936–7942.